Sensors and Actuators B 200 (2014) 288–296

Contents lists available at ScienceDirect

Sensors and Actuators B: Chemical

journal homepage: www.elsevier.com/locate/snb

Highly sensitive and selective triethylamine-sensing properties of nanosheets directly grown on ceramic tube by forming NiO/ZnO PN heterojunction

Dianxing Ju[a,b], Hongyan Xu[a,b], Zhiwen Qiu[a,b], Jing Guo[a,b], Jun Zhang[a,b], Bingqiang Cao[a,b,*]

[a] Key Laboratory of Inorganic Functional Materials in Universities of Shandong, School of Materials Science and Engineering, University of Jinan, Jinan 250022, Shandong, China
[b] Shandong Provincial Key Lab of Preparation and Measurement of Building Materials, University of Jinan, Jinan 250022, China

ARTICLE INFO

Article history:
Received 5 February 2014
Received in revised form 7 April 2014
Accepted 10 April 2014
Available online 24 April 2014

Keywords:
ZnO nanosheets
NiO
PN heterojunction
TEA sensor
Depletion layer

ABSTRACT

Chemiresistive gas sensors with high sensitivity, selectivity and reliable fabrication potency for specific gas have been now expected for many applications. A highly sensitive and selective nanostructured triethylamine (TEA) gas sensor has been fabricated successfully by designing PN heterojunction consisting of ZnO nanosheets and NiO nanoparticles. The ZnO nanosheets directly grew on Al_2O_3 ceramic tubes by introducing a seed layer with a simple and cost-effective hydrothermal method. By employing pulsed laser deposition (PLD) method, the construction of NiO/ZnO PN heterojunction is highly controllable and reproducible. In comparison with ZnO nanosheet, the NiO/ZnO nanoparticle/nanosheet heterojunction exhibits much better sensing property to TEA gas. The depletion layer formed at the PN junction interface in NiO/ZnO sensor can greatly increase the resistance in air and decrease the resistance in TEA gas. Due to the general working principle and controllable growth strategy, this study provides a way for design and fabrication of the chemiresistive gas sensors with high performance.

1. Introduction

As one of explosive and inflammable gases, triethylamine (TEA) is widely used as organic solvents, preservatives, catalysts and synthetic dyes [1,2]. TEA is also secreted in dead fish and sea creatures and the concentration increases with the decay of the dead fish and marine products. It can cause great damage on human health like skin burns, headaches, nausea, eye irritation and especially respiratory difficulty due to strong pungency with result of pulmonary edema and even death [1]. Many evidences indicated that it may also endanger our environment by forming explosive mixture when its steam mixes with air and even causes combustion once the TEA is exposed to flame. Several methods have been adopted to detect triethylamine, such as gas/liquid/film chromatography, electrochemistry analysis, and colorimetric method [3–5]. Although these traditional methods are effective for TEA detection, some disadvantages are also clear. For example, electrochemistry analysis always needs reference electrodes and other chromatography methods typically require expensive equipment [6,7]. Thus, accurate and fast detection of TEA especially with high sensitivity and good selectivity is always in great demand in biomedical, chemical and food industries and also useful in our daily life [6].

ZnO is a chemically and thermally stable n-type oxide semiconductor with wide band gap energy of 3.37 eV at room temperature [8–10]. It is one of the most intensively studied materials owing to its variable important potential applications [11,12]. One-dimensional (1D) ZnO nanostructures like nanowires [13], nanotube [14] and nanobelts [15] have been demonstrated for sensor applications with high sensitivity due to their large surface area, less agglomerated configuration and high crystallinity [16,17]. In particular, the gas response will be enhanced when the diameter of 1D nanostructures is similar to the dimension of the electron depletion layer [18,19]. 1D ZnO nanowire-based sensors are usually fabricated via “pick and place” method like photolithography, followed by a series of tedious processes involving synthesis, sonication, and dispersal of ensemble nanowires on another substrate with prefabricated electrodes [20]. However, these cannot be used for wide practical applications because of the power-consuming and low-yield process. Bie et al. [21] directly

* Corresponding author at: University of Jinan, MSE, Nanxinzhuang West Raod 336, Jinan 250022, China. Tel.: +86 531 8973 6292; fax: +86 531 8797 4453.
E-mail address: mse_caobq@ujn.edu.cn (B. Cao).

http://dx.doi.org/10.1016/j.snb.2014.04.029
0925-4005/

synthesized ZnO nanorod arrays on Al_2O_3 tube through a solution method, which simplified the traditional slurry-coating process of sensor fabrication. However, due to the poor contacts between the vertical nanorods, the transport of electrons was limited, which increased the device resistance and reduced the sensor sensitivity. Two-dimensional (2D) nanostructures such as ZnO nanoplates [22] and nanosheets [23] have provided good opportunities to overcome these disadvantages. From the practical application point of view, ZnO nanosheet networks are extremely interesting because of their large surface areas and better conductivity, which have been demonstrated as sensors [23], solar cells [24], UV photodetectors [25], and field emission devices [26]. In comparison with 1D nanowire, the 2D ZnO nanostructure is much more difficult to grow partially due to its hexagonal polar structure. Till now, only a few papers have reported the growth of ZnO nanosheets. Rahm et al. [27] synthesized the ZnO nanosheet networks via the vapor–liquid–solid (VLS) mechanism. Recently, Zhang et al. [28] prepared porous ZnO nanosheets with a hydrothermal method and demonstrated their ethanol response through the traditional slurry-coating gas sensor fabrication process. Therefore, synthesis of 2D ZnO nanostructure directly onto the generally used alumina ceramic Al_2O_3 tubes and exploration of their sensor applications are still in the early stage.

Previous reports have demonstrated that ZnO nanostructure based gas sensors exhibit good response to many toxic gases like trimethylamine (TMA) [29], CO and NH_3 [30]. However, gas sensors for detecting TEA are rarely reported. To the best of our knowledge, only Wang et al. fabricated SnO_2 nanorods sensor with the traditional slurry-coating method to detect TEA and the response to 1000 ppm TEA was only 200 when operating at 350 °C [31]. Then, Lv et al. prepared ZnO nanorod gas sensor with the same method and the response was enhanced from 300 to 500 ppm TEA gas [32]. Recently, some papers have reported that noble metal particles sensitized semiconductor and formation of semiconductor heterojunction both can improve the sensor sensitivity and/or selectivity. For example, our group prepared Au nanoparticles-functionalized ZnO nanoplates via a facile one-pot hydrothermal method and the sensor exhibited faster response–recovery time and higher response compared with the pristine ZnO sensor [33]. Kim et al. fabricated CuO–ZnO composite hollow spheres for H_2S gas sensor and enhanced response was also demonstrated in comparison with pure ZnO hollow spheres [34].

In this paper, we first synthesize ZnO nanosheet by a simple hydrothermal method on ordinary Al_2O_3 ceramic tubes with predesigned electrodes, which can be used directly for gas sensor fabrication without the slurry-coating fabrication process. In order to improve the sensing performance, we design a ZnO/NiO heterojunction sensor to detect TEA gas, where NiO nanoparticles were implanted onto the surface of ZnO nanosheets by pulsed laser deposition (PLD). NiO is an oxide semiconductor with a bandgap of 4.2 eV and has been used in different optoelectronic devices due to its easily controllable p-type conductivity [35–37]. With the formation of PN heterojunction, the sensitivity and selectivity of ZnO/NiO nanosheet sensors was enhanced obviously in comparison with pure ZnO nanosheet sensor and the sensing mechanism was also discussed.

2. Experimental

2.1. Direct growth of ZnO nanosheets on Al_2O_3 ceramic tubes

All the chemicals were purchased from Sinopharm Chemical Reagent (Shanghai, China). ZnO nanosheets were synthesized by a hydrothermal method. The typical process is briefly described as follows. 4.4 g $Zn(Ac)_2$ was dissolved in 25 ml 2-methoxyethanol under stirring and 1.2 ml ethanolamine was added into the solution after $Zn(Ac)_2$ was completely dissolved, and then we got the ZnO sol. After that, cleaned Al_2O_3 tubes with predesigned gold electrodes on two ends were immersed into the ZnO sol for 4 h and then annealed at 350 °C for 30 min to form ZnO seeds layer. Mixed aqueous solution of 0.025 M zinc nitrate and 0.025 M hexamethylenetetramine ($C_6H_{12}N_4$) were transferred into Teflon-lined stainless steel autoclaves. At the same time, the Al_2O_3 tubes were suspended into the aqueous solution. After the reaction at 95 °C for 8 h, we got ZnO nanosheet samples. Finally, they were rinsed with deionized water and ethanol several times and dried with pure nitrogen.

2.2. Growth of NiO nanoparticles onto ZnO nanosheets by PLD

A layer of NiO nanoparticles was deposited onto the surface of ZnO nanosheets by pulsed laser deposition (PLD) using NiO target at room temperature. A KrF laser of 1 mJ/cm^2 and an oxygen partial pressure of 3×10^{-4} Pa were typically applied. By controlling the laser pulses, e.g., 1000, 3000, 5000 pulses, the NiO/ZnO nanosheet heterojunction with NiO nanoparticle layer of different thickness were grown. Thus, different gas sensors directly fabricated with ZnO nanosheets, named as ZS sensor, and ZnO/NiO nanosheet heterojunction, named as ZNS sensor, were ready for further measurement.

2.3. Material characterizations and sensor properties

The morphology and composition of the sensors were measured by a field emission scanning electron microscope (FESEM, FEI QUANTA FEG250) equipped with an energy dispersive X-ray spectroscopy (EDS, INCA MAX-50) and a high-resolution transmission electron microscope (HRTEM, JEM-2100F, JEOL). The phase of the sensor materials was checked with X-ray diffraction (XRD, D8-Advance, Bruker). The gas sensor properties were measured by a gas sensing test system (WS-30A, Weisheng Electronics, Zhengzhou, China). The devices were put into an airproof test box. Test gases such as TEA and ethanol with calculated concentration were injected into the testing chamber by a microsyringe. The sensor response is defined as the ratio of R_a/R_g, where R_a and R_g are the resistances of the sensors in air and in target gas, respectively. The response and recovery time was defined as the time needed for the sensor-resistance to change by 90% of the difference from the maximum after injecting and removing the detected gas.

3. Results and discussion

3.1. Characterizations of ZnO and ZnO/NiO nanosheets

The morphology of the ZnO and NiO/ZnO nanosheet is characterized with SEM and TEM microscopes. Fig. 1(a) is an optical photograph of an Al_2O_3 tube gas sensor of ZnO nanosheet, interdigitated with a pair of Au electrodes, Pt lead wires and heater. The surface morphology of the ZnO nanosheets is shown in Fig. 1(b). Most of the nanosheets stand vertically on the substrate and the thickness is uniform and homogenous. At the same time, the nanosheets interconnect each other and form an open network with large surface area that could increase the adsorption sites and contribute to the adsorption of target gas molecules. Fig. 1(c) presents a TEM image for an isolated ZnO nanosheet. The inset SAED pattern indicates that the nanosheet is of polycrystalline structure composed of small particles at nanoscale. Fig. 1(d) shows the same HRTEM image, where the lattice spacings of few nanoparticles are determined to be 0.28 nm and 0.25 nm, corresponding to the $\{0\,1\,-1\,0\}$ and $\{1\,0\,-1\,1\}$ planes of the wurtzite ZnO. Fig. 1(e) shows that the ZnO nanosheet morphology is still stable when it

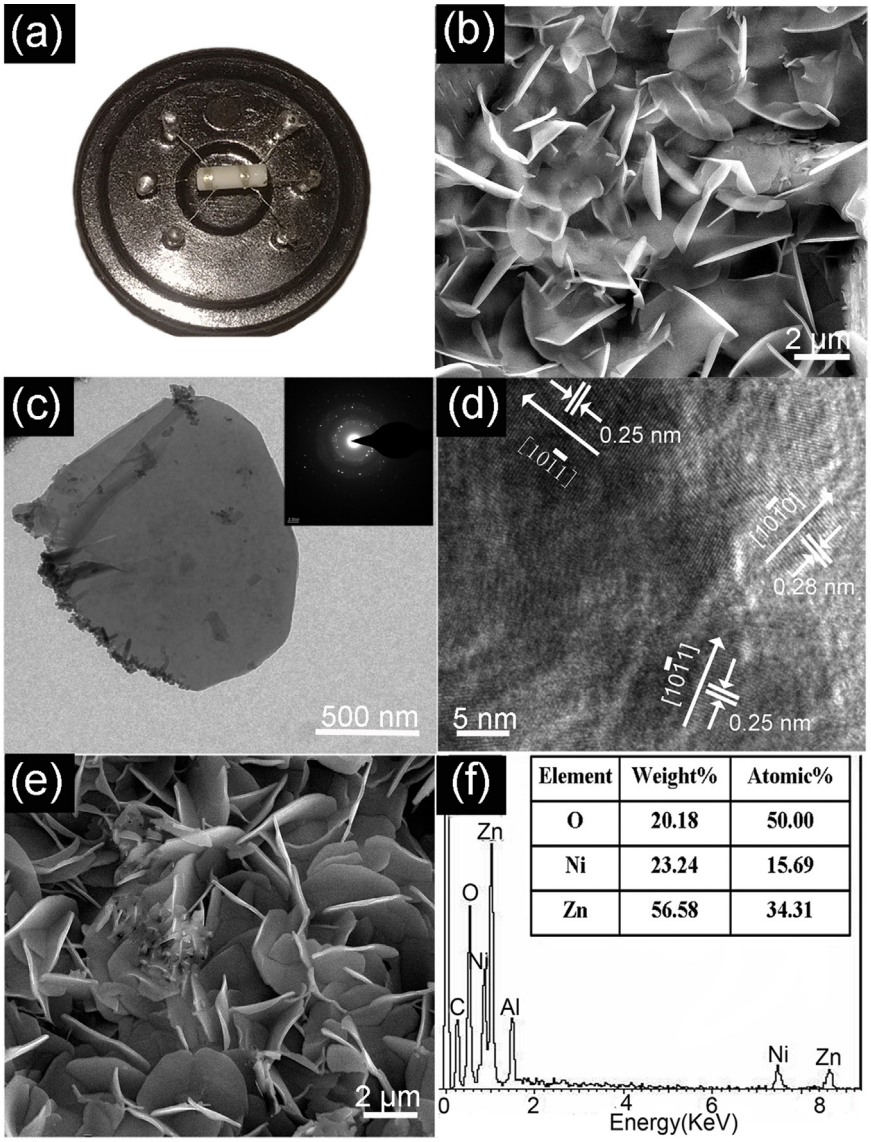

Fig. 1. (a) Gas sensor of ZnO nanosheets fixed on an electronic bracket; (b) SEM image of two-dimensional ZnO nanosheets taken from (a); ((c) and (d)) TEM and HRTEM images of ZnO nanosheets taken from (a), inset of (c) is a corresponding SAED pattern; (e) SEM image of ZnO nanosheets after a PLD growth process for NiO and (f) the corresponding EDS spectra of the sample shown in (e).

was covered with a thin layer of NiO nanoparticles onto their surface by PLD. Fig. 1(f) is the EDS spectrum of the NiO/ZnO nanosheet. The peak of Ni can be clearly observed in the spectrum. The peak of Al also can be observed in the spectrum, which is attributed to the direct growth of the ZnO nanosheets on the Al_2O_3 tube.

The phases of the as-synthesized ZnO and ZnO/NiO composite sample were confirmed by XRD. Fig. 2(a) shows the XRD spectrum of the ZnO nanosheets. Typical wurtzite ZnO (JCPDS Card No. 36-1451) diffraction patterns can be observed together with the diffraction peaks of under Al_2O_3 substrate. After the further calcination at 320 °C, no detectable phase change was observed for ZnO nanosheets. When NiO was implanted onto ZnO nanosheets, the week peeks from NiO (JCPDS card No. 78-0643) due to small amount were also observed.

3.2. Performance comparison of ZS and ZNS sensors

The gas sensing properties of ZS and ZNS sensors were first measured at different working temperatures. Fig. 3 shows the response of the sensors to 100 ppm TEA, as a function of the working

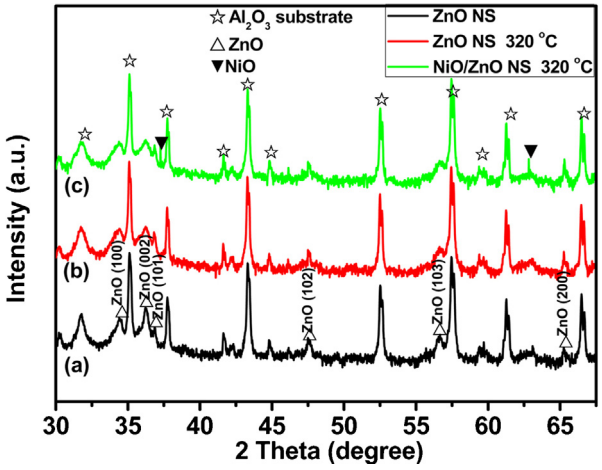

Fig. 2. XRD spectra of as-synthesized (a) ZnO nanosheet grown on Al_2O_3 substrate. (b) ZnO nanosheet and (c) NiO/ZnO nanosheet after heating at the sensor working temperature of 320 °C.

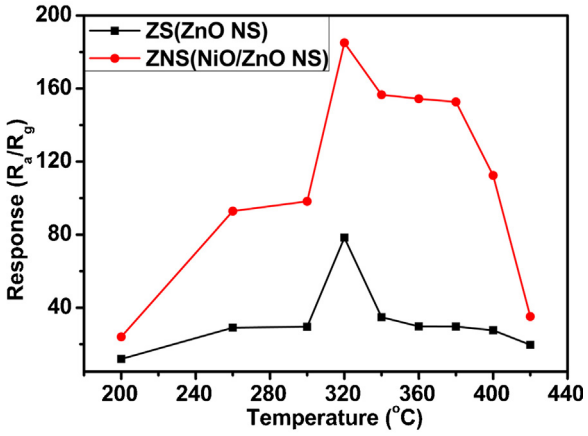

Fig. 3. The relationship between working temperature and response of ZnO sensor (ZS sensor) and NiO/ZnO sensor (ZNS sensor) to 100 ppm TEA gas.

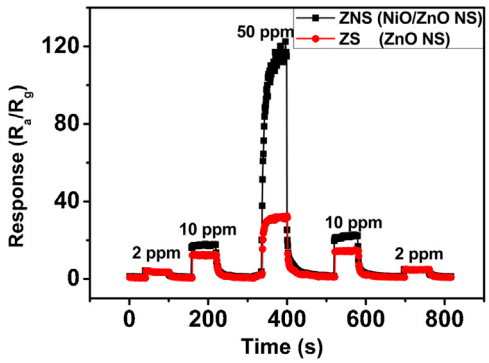

Fig. 4. Response comparison of ZnS sensor and ZNS sensor to TEA gas of different concentrations at 320 °C.

temperature in a range of 200–420 °C. The optimal operating temperature for our sensors is around 320 °C and the response of ZNS sensor is much higher than that of ZS sensor in the whole temperature range. When the temperature is 200 °C, the sensors response can reach to 11.9 (ZS sensor) and 24.1 (ZNS sensor). Furthermore, with the increase of working temperature, the response further increases. Until the temperature is up to 320 °C, both of the two sensors exhibit the maximum response of 78.4 (ZS sensor) and 185.1 (ZNS sensor), respectively. Then, the response decreases as the temperature further increases, which is due to the competing desorption of the chemisorbed oxygen [21].

Fig. 4 shows the response curve of ZNS sensor to TEA of different concentrations from 2 ppm to 50 ppm at 320 °C. ZNS sensor response increases with the increasing concentration of TEA and also exhibits good repeatability. The ZNS sensor response increases gradually and can get up to 130 when the TEA concentration is 50 ppm. It also indicates that the detection limit could be down to 2 ppm-level with a response of 3.2. Fig. 5(a) and (b) compares the response and recovery time of the ZS sensor and ZNS sensor to 10 ppm TEA at 320 °C, which are also vital characteristic parameters for gas sensors. It can be clearly observed that when the target gas was injected into the box, both of the two sensors response fast and their response time is 6–7 s, respectively. After desorption, ZNS sensor needs longer time to recover to a low voltage state than ZS sensor.

The cross response properties of the two sensors were examined by exposing ZS sensor and ZNS sensor to 100 ppm TEA and other gases like ethanol, acetone, 2-propanol, *p*-xylene, C_6H_6, C_6H_{12}, CH_3OH and *n*-hexane of same concentration at 320 °C, as summarized in Fig. 6(a). The ZNS sensor exhibit response lower than 20 to those interfering gases except ethanol. But, the response to TEA is as high as 185. This indicates an excellent selectivity to TEA. Moreover, the ZNS sensor response values are all higher than those of ZS sensor, especially to TEA. The maximum response of ZNS sensor to TEA is about 2.3 times higher than the pure ZnO nanosheets sensor. The enhancement of response can be attributed to the formation of PN heterojunction. The stability of the two sensors over one month was also checked as shown in Fig. 6(b). Clearly, the sensors show a nearly constant response to 100 ppm TEA, which indicates a high stability of the sensor devices. Moreover, another nine ZnO/NiO sensors were assembled to check the reproducibility of different sensors and the data is shown in Fig. 7. It can be seen that five sensors show higher response 150–200, two sensors show response of 100–150 and two sensors show response of 50–100, which exhibit a relative good reproducibility for different ZNS sensors.

3.3. Mechanism on enhanced ZNS sensing properties

The sensing mechanism of n-type semiconductor sensors has been well documented with the space–charge or depletion layer model [38–40]. The adsorption and desorption of the target gas molecules on the surface of sensing materials can effectively cause the change of resistance. This is the basic working principle of oxide semiconductor sensor like pure ZnO nanosheet sensor, and the working principle in air and target gas are schematically shown in Fig. 8(a–d). However, when the PN heterojunction was formed at the interface of oxide semiconductors with different conductivity types, the sensing mechanism will be different. Although their enhanced sensing properties were

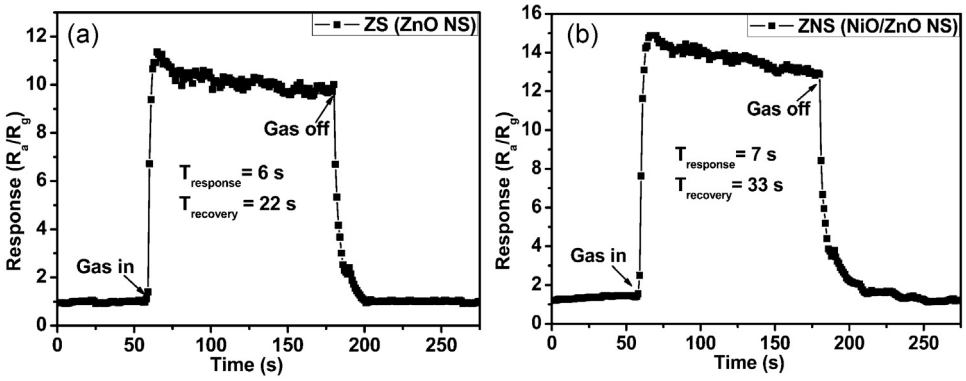

Fig. 5. Response and recovery time of the ZS and ZNS sensors to 10 ppm TEA at 320 °C. (a) ZS sensor, (b) ZNS sensor.

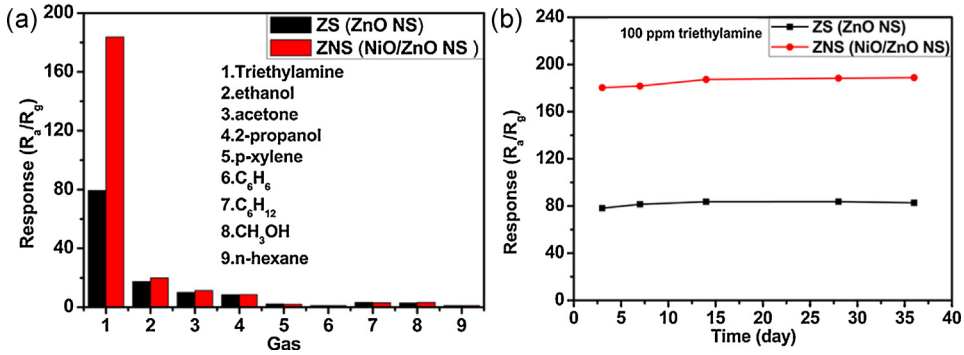

Fig. 6. (a) The cross-response of ZS and ZNS sensors to 100 ppm TEA and other interfering gases at 320 °C; (b) Long-term stability of the ZS and ZNS sensors to 100 ppm TEA at 320 °C.

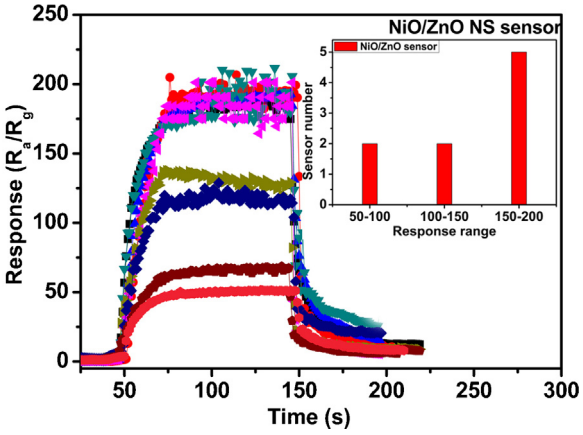

Fig. 7. The reproducibility of nine ZNS sensors to 100 ppm TEA at 320 °C.

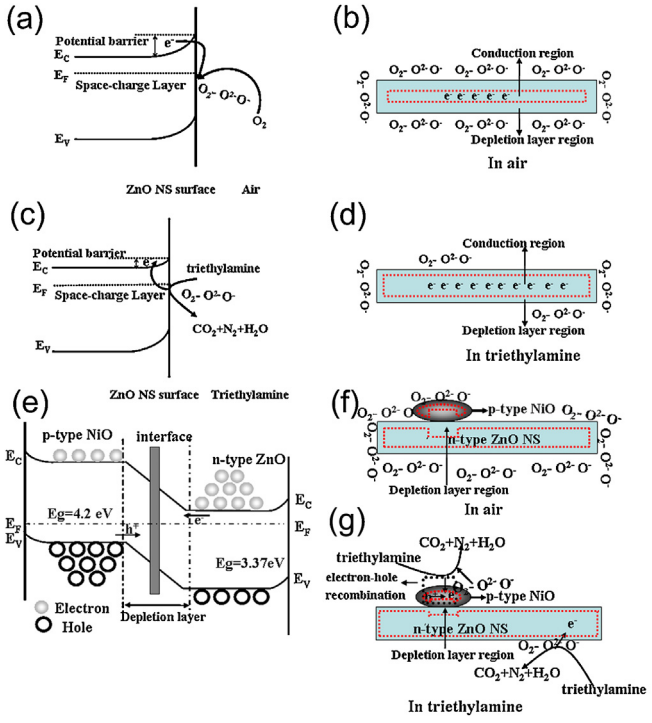

Fig. 8. ((a) and (b)) The energy band diagram of ZnO nanosheet and its schematic model in air; ((c) and (d)) The energy band diagram of ZnO nanosheet and its schematic model in TEA; (e) The energy band diagram of p-type NiO and n-type ZnO heterostructure; ((f) and (g)) schematic model for the ZNS sensor exposed to air and TEA gas, respectively. The out parts indicated by red dashed lines are the depletion layers. (For interpretation of the references to color in this figure legend, the reader is referred to the web version of this article.)

reported [41–48], the gas sensing mechanism remains unclear [42,43,48].

As we all know, the majority carriers of n-type and p-type semiconductors are electrons and holes, respectively. Thus ZnO mainly shows n-type conductivity by electrons and NiO displays p-type conductivity by holes. When NiO nanoparticles are implanted onto the surface of ZnO nanosheet, the electrons in ZnO and holes in NiO diffuse in opposite direction due to the great gradient of the same carrier concentration. Then, an internal built-in electric field is induced at the ZnO/NiO interface and the carriers diffuse are finally balanced. As a result, the energy band bends in the depletion layer until the system gets a uniform Fermi level (E_F). This is the formation of PN junction in thermal equilibrium, as shown in Fig. 8(e). When pure ZnO nanosheets are exposed to air at a high temperature, a depletion layer will form on the surface of ZnO nanosheet due to the adsorption of oxygen molecules, leading to the high resistance state of sensing materials, as shown in Fig. 8(a and b). Moreover, the formation of NiO/ZnO PN junction with a new depletion layer at their interface also make sensor's resistance to further increase in air, as illustrated in Fig. 8(f). However, once the ZNS sensor is exposed to reducing TEA gas, TEA reacts with the oxygen ions absorbed on the surface of ZnO nanosheets and releases the electrons back to the ZnO. So, the resistance of the sensor decreases. In addition, TEA releases electrons into p-type NiO and the electron–hole recombination leads to a decrease of holes concentration. According to the law of mass action ($n_0 \times p_0 = n_i^2$) for semiconductor, the decrease of holes in NiO results in the increase of electrons and reduces the concentration gradient of the same carriers on both sides of PN junction. Consequently, the diffusion of carriers is weakened and the depletion layer at the interface becomes thin. Therefore, the resistance of the ZNS sensor in TEA is further decreased. Fig. 8(g) displays a model for ZNS sensor when exposed to TEA gas. In brief, in comparison with the ZS sensor, the formation of PN junction in ZNS sensor greatly increases the resistance in air and decreases the resistance in TEA gas. Thus, based on the definition of sensor response ($S = R_a/R_g$), the enhanced S to TEA is mainly attributed to the variation of resistance caused by the formation of PN junction. This theoretical model can also be used to explain other materials systems with their response improved by heterojunction, such as CuO–SnO_2 [44] and NiO–SnO_2 [45].

In addition, the different reaction activity of target gases in terms of bond energy maybe another reason for the different enhancement of ZNS gas sensing property [49,50]. The main bond energy of measured target gas, e.g., TEA (C—N), hexane (C—C), benzene (C=C), acetone (C=O), and ethanol/methanol (O—H), are 307, 345, 610.3, 798.9, 458.8 kJ/mol, respectively [50]. Due to the low C—N bond energy (307 kJ/mol), the high reaction activity of TEA molecule is also expected to contribute to the high response of ZNS sensors.

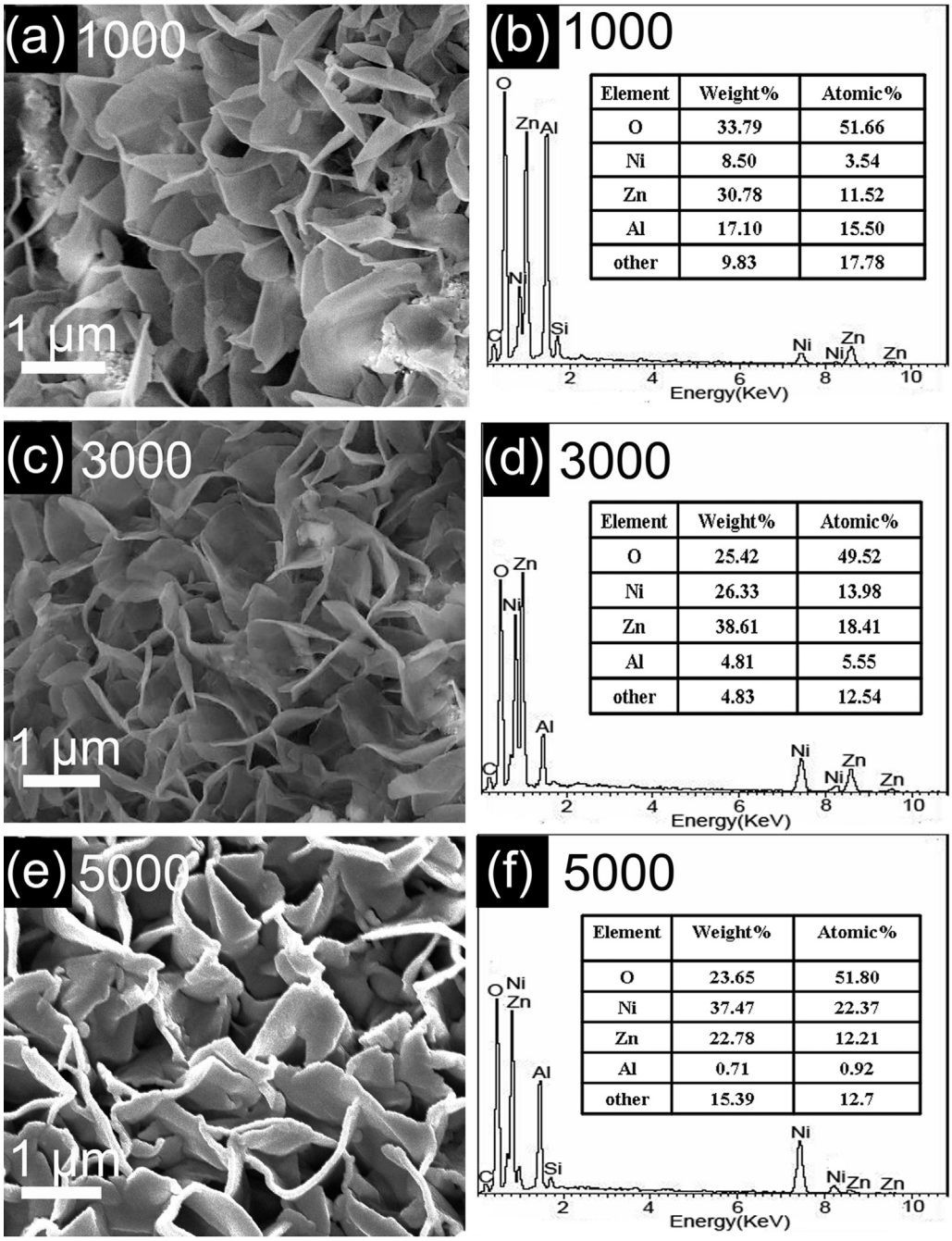

Fig. 9. SEM images and the corresponding EDS spectra of ZnO nanosheets after a PLD growth process for NiO with different deposition laser pulses. ((a) and (b)) 1000 pulses, ((c) and (d)) 3000 pulses, ((e) and (f)) 5000 pulses.

3.4. More proof on ZNS sensing mechanism

To further prove the above ZNS sensing mechanism, we investigated the influence of NiO nanoparticle layer thickness on their sensing property by controlling the laser pulses. Fig. 9(a), (c) and (e) shows the SEM images of ZnO nanosheets samples after NiO nanoparticles deposition with laser pulses of 1000, 3000, 5000 times, respectively. It can be clearly seen that ZnO nanosheets become a little thicker with the deposited NiO increase. Fig. 9(b), (d) and (f) is the corresponding EDS spectrum of the NiO/ZnO samples. The peak of Ni can be all clearly observed in the spectra. According to the EDS analysis shown in inset of Fig. 9(b, d and f), the specific content of each element is listed in the table, which further indicates the increase of NiO when more laser pulses were applied.

Fig. 10 shows the response of the three ZNS sensors to 100 ppm TEA as a function of the working temperature in the range of 260–400 °C. The response of three ZNS sensors got the maximum at temperature up to 320 °C, and then decreased as the temperature further increased. Fig. 11(a) is the isothermal response curve to TEA of different concentrations from 2 to 100 ppm at 320 °C. The ZNS sensors response first increases with applied laser pulse and then decreases when the laser pulse is over 5000. The ZnO nanosheet sensor with NiO deposited by 3000 laser pulses (named as ZNS3) shows the maximum response than other two in the whole temperature range. This observed phenomena can be well understood based on the above proposed sensing mechanism. With the deposition laser pulses increasing from 1000 to 3000, the sensitivity of the ZNS sensors are enhanced obviously which is mainly due to the

Table 1
Sensing properties of ZnO nanosheets and other reported oxide semiconductor gas sensors working under different operating temperatures.

Material	Gas concentration (ppm)	Operating temperature (°C)	Sensitivity (R_a/R_g)	$T_{response}$ (s)	$T_{recovery}$ (s)
SnO_2 nanorods [32]	1000 (TEA)	350	200	10	10
ZnO nanorods [33]	500 (TEA)	150	300	15	15
SnO_2 flowerlike [2]	100 (TEA)	350	4	<6	<6
$NiFe_2O_4$ nanorods [53]	100 (TEA)	175	100	22	–
SnO_2–ZnO nanocomposite [3]	100 (TMA)	330	200	10	30
ZnO film [54]	400 (TMA)	300	3.5	–	–
ZnO film [55]	160 (TMA)	300	60	–	–
Our work	100 (TEA)	320	300	7	33

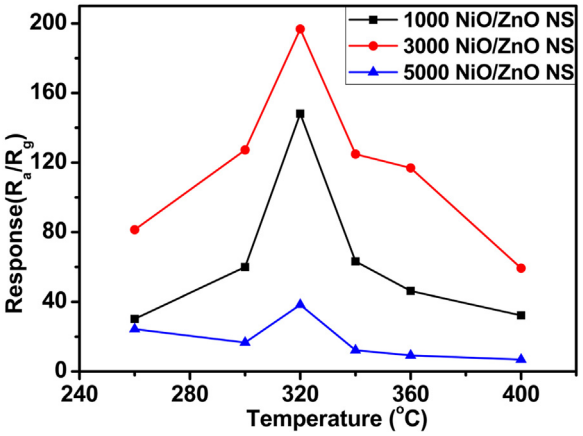

Fig. 10. The relationship between the response and working temperature of ZNS sensors with NiO layer of different thickness to 100 ppm TEA gas.

increase of the PN junction number. But when the deposition laser pulses increase to 5000, the surface of ZnO nanosheet is covered with more NiO nanoparticles and the gas adsorption sites of n-type ZnO to TEA is greatly reduced. As a result, the target gas molecules mainly react with p-type NiO rather than n-type ZnO nanosheet with a result of low response. So, the theoretical PN heterojunction sensing model was further verified by changing of the number of NiO nanoparticles on the same ZnO nanosheets surface.

For the optimized ZnO/NiO heterostructure, the ZNS3 sensor got a response of 42 to 2 ppm TEA gas. With the increase of TEA concentration, the sensor response shows a clear increase as shown in Fig. 11(b). Generally, the relation between gas concentration and the response of metal oxide semiconductor gas sensor can be described with an empirical formula as

$$S = K_a[C]^{K_b} + 1 \quad \text{or} \quad \log(S-1) = K_b \log(C) + \log K_a$$

where K_a and K_b are constants and C is the concentration of the target gas [51]. In our work, the response exhibits a good linear relationship with the concentration in a logarithm scale, as shown in Fig. 12(a). Therefore, the detection limit of the sensor even could be

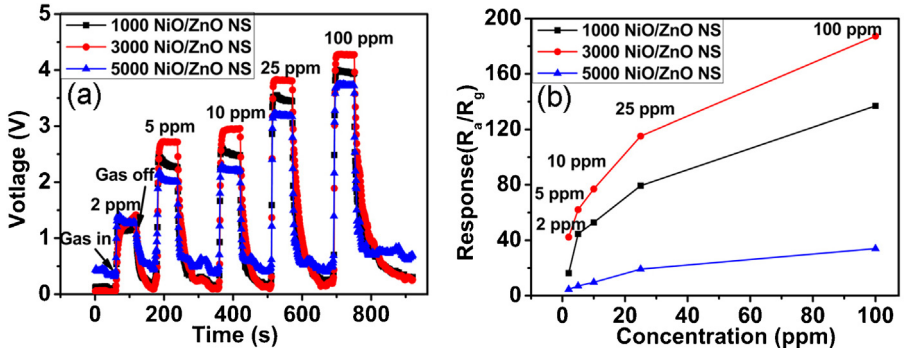

Fig. 11. (a) Responses of three ZNS sensors to TEA of different concentrations at 320 °C, (b) the corresponding relationship between response and concentration.

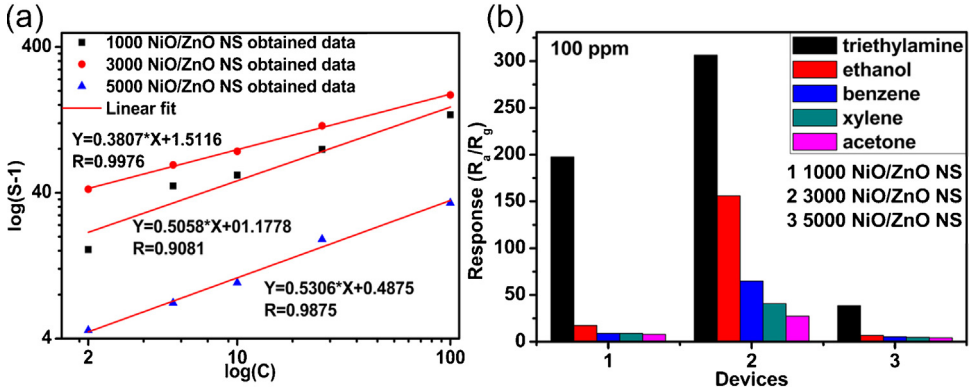

Fig. 12. (a) The $\log(S-1)$ versus $\log(C)$ plot of three ZNS sensors for TEA gas and the corresponding linearly fitted results; (b) selectivity of three ZNS sensors for different target gases aged two weeks.

down to ppb-level [52]. To further check the heterojunction sensing properties, the ZNS sensor selectivity was measured after aging for two weeks, as shown in Fig. 12(b). After aging, the response of these sensors is enhanced and exhibits good selectivity to TEA. This is very attractive for trace TEA detection. A comparison between the sensing performances of our sensor and literature results is summarized in Table 1. It is worth noting that the ZNS3 sensor fabricated in our work exhibits the highest response in comparison with those reported in the literature.

4. Conclusions

In conclusion, we report a highly sensitive and selective NiO/ZnO PN heterojunction TEA gas sensor and the sensing mechanism is also discussed in detail. By introducing a seed layer, ZnO nanosheets directly grew on Al_2O_3 ceramic tube with a simple and cost-effective hydrothermal method. By employing PLD method, the construction of NiO/ZnO PN heterojunction is highly controllable and reproducible. The NiO/ZnO nanosheet gas sensor exhibits highly sensitive and selective sensing property to TEA gas. The as-prepared sensor response could get up to 185 and then 300 after two weeks aging when exposed to 100 ppm TEA, which is much higher than that of pure ZnO nanosheet sensor and other reported oxide chemiresistive gas sensors. In comparison with the ZS sensor, the depletion layer formed at the PN heterointerface in ZNS sensor greatly increases the resistance in air and decreases the resistance in TEA gas. Thus, the enhanced response to TEA is mainly attributed to the variation of resistance caused by the formation of PN junction. This theoretical model was further proved by optimization of NiO/ZnO heterostructure and can also be used to explain other heterojunctions for sensor application. This study provides a rational way for design and fabrication of the chemiresistance gas sensors with high performances.

Acknowledgments

This work is supported by NSFC (11174112) and Shandong Provincial Science Foundation (JQ201214, BS2012CL003). The research programs from Ministry of Education of the People's Republic of China, are also acknowledged (NCET-11-1027, 213021A). BC thanks the Taishan Scholar Professorship (TSHW20091007) tenured at University of Jinan.

References

[1] L. Xu, H.J. Song, J. Hu, Y. Lv, K.L. Xu, A cataluminescence gas sensor for triethylamine based on nanosized LaF_3–CeO_2, Sens. Actuators, B: Chem. 169 (2012) 261–266.
[2] B. Liu, L.H. Zhang, H. Zhao, Y. Chen, H.Q. Yang, Synthesis and sensing properties of spherical flowerlike architectures assembled with SnO_2 submicron rods, Sens. Actuators, B: Chem. 173 (2012) 643–651.
[3] W.H. Zhang, W.D. Zhang, Fabrication of SnO_2–ZnO nanocomposite sensor for selective sensing of trimethylamine and the freshness of fishes, Sens. Actuators, B: Chem. 134 (2008) 403–408.
[4] W.M. Moore, R.J. Edwards, L.T. Bavda, An improved capillary gas chromatography method for triethylamine: application to sarafloxacin hydrochloride and GnRH residual solvents testing, Anal. Lett. 32 (1999) 2603–2612.
[5] J.F. Haskin, G.W. Warren, L.J. Priestley, Gas chromatography determination of constituents in the study of azeotropes, Anal. Chem. 30 (1958) 217–219.
[6] E. Filippo, D. Mannob, A. Buccolieri, A. Serra, Green synthesis of sucralose-capped silver nanoparticles for fast colorimetric triethylamine detection, Sens. Actuators, B: Chem. 178 (2013) 1–9.
[7] H. Nohta, H. Satozono, K. Koiso, H. Yoshida, J. Ishida, M. Yamaguchi, Highly selective fluorometric determination of polyamines based on intramolecular excimer-forming derivatization with a pyrene-labeling reagent, Anal. Chem. 72 (2000) 4199–4204.
[8] J. Kim, K. Yong, Mechanism study of ZnO nanorod bundle sensors for H_2S gas sensing, J. Phys. Chem. C 115 (2011) 7218–7224.
[9] Y.H. Xiao, L.Z. Lu, A.Q. Zhang, Y.H. Zhang, L. Sun, L. Huo, F. Li, Highly enhanced acetone sensing performances of porous and single crystalline ZnO nanosheets: high percentage of exposed (1 0 0) facets working together with surface modification with Pd nanoparticles, ACS Appl. Mater. Interfaces 4 (2012) 3797–3804.
[10] H.Y. Xu, X.L. Liu, D.L. Cui, M. Li, M.H. Jiang, A novel method for improving the performance of ZnO gas sensors, Sens. Actuators, B: Chem. 114 (2006) 301–307.
[11] C. Soldano, E. Comini, C. Baratto, M. Ferroni, G. Faglia, G. Sberveglieri, Metal oxides mono-dimensional nanostructures for gas sensing and light emission, J. Am. Ceram. Soc. 95 (2012) 831–850.
[12] X.H. Zhang, M.X. Huang, Y.J. Qiao, Synthesis of SnO_2 single layered hollow microspheres and flowerlike nanospheres through a facile template-free hydrothermal method, Mater. Lett. 95 (2013) 67–69.
[13] S. Park, S. An, H. Ko, C. Jin, C. Lee, Synthesis of nanograined ZnO nanowires and their enhanced gas sensing properties, ACS Appl. Mater. Interfaces 4 (2012) 3650–3656.
[14] Y.J. Chen, C.L. Zhu, G. Xiao, Ethanol sensing characteristics of ambient temperature sonochemically synthesized ZnO nanotubes, Sens. Actuators, B: Chem. 129 (2008) 639–642.
[15] C.W. Na, S.Y. Park, J.-H. Lee, Punched ZnO nanobelt networks for highly sensitive gas sensors, Sens. Actuators, B: Chem. 174 (2012) 495–499.
[16] D. Zhang, S. Chava, C. Berven, S.K. Lee, R. Devitt, V. Katkanant, Experimental study of electrical properties of ZnO nanowire random networks for gas sensing and electronic devices, Appl. Phys. A 100 (2010) 145–150.
[17] L.W. Wang, Y.F. Kang, X.H. Liu, S.M. Zhang, W.P. Huang, S.R. Wang, ZnO nanorod gas sensor for ethanol detection, Sens. Actuators, B: Chem. 162 (2012) 237–243.
[18] M.H. Xu, F.S. Cai, J. Yin, Z.H. Yuan, L.J. Bie, Facile synthesis of highly ethanol-sensitive SnO_2 nanosheets using homogeneous precipitation method, Sens. Actuators, B: Chem. 145 (2010) 875–878.
[19] L.X. Zhang, Y.Y. Yin, Hierarchically mesoporous SnO_2 nanosheets: hydrothermal synthesis and highly ethanol-sensitive properties operated at low temperature, Sens. Actuators, B: Chem. 185 (2013) 594–601.
[20] Y. Huang, X. Duan, C.M. Lieber, Nanowires for integrated multicolor nanophotonics, Small 1 (2004) 142–147.
[21] L.J. Bie, X.N. Yan, J. Yin, Y.Q. Duan, Z.H. Yuan, Nanopillar ZnO gas sensor for hydrogen and ethanol, Sens. Actuators, B: Chem. 126 (2007) 604–608.
[22] Z.H. Jing, J.H. Zhan, Fabrication and gas-sensing properties of porous ZnO nanoplates, Adv. Mater. 20 (2008) 4547–4551.
[23] Y. Zeng, L. Qiao, Y.F. Bing, M. Wen, B. Zou, W.T. Zheng, T. Zhang, G.T. Zou, Development of microstructure CO sensor based on hierarchically porous ZnO nanosheet thin films, Sens. Actuators, B: Chem. 173 (2012) 897–902.
[24] J.H. Qiu, M. Guo, X.D. Wang, Electrodeposition of hierarchical ZnO nanorod–nanosheet structures and their applications in dye-sensitized solar cells, ACS Appl. Mater. Interfaces 3 (2011) 2358–2367.
[25] B.Q. Cao, T. Matsumoto, M. Matsumoto, M. Higashihata, D. Nakamura, T. Okada, ZnO nanowalls grown with high-pressure PLD and their applications as field emitters and UV detectors, J. Phys. Chem. C 113 (2009) 10975–10980.
[26] B.Q. Cao, W.P. Cai, From ZnO nanorods to nanoplates: chemical bath deposition growth and surface-related emissions, J. Phys. Chem. C 112 (2008) 680–685.
[27] A. Rahm, G.W. Yang, M. Lorenz, T. Nobis, J. Lenzner, G. Wagner, M. Grundmann, Two-dimension al ZnO:Al nanosheets and nanowalls obtained by Al_2O_3-assisted carbothermal evaporation, Thin Solid Films 486 (2005) 191–194.
[28] L.X. Zhang, J.H. Zhao, H.Q. Lu, L. Li, J.F. Zheng, H. Li, Z.P. Zhu, Facile synthesis and ultrahigh ethanol response of hierarchically porous ZnO nanosheets, Sens. Actuators, B: Chem. 161 (2012) 209–215.
[29] Z. Lou, F. Li, J.N. Deng, L.L. Wang, T. Zhang, Branch-like hierarchical heterostructure (α-Fe_2O_3/TiO_2): a novel sensing material for trimethylamine gas sensor, ACS Appl. Mater. Interfaces 5 (2013) 12310–12316.
[30] W. An, X.J. Wu, X.C. Zeng, Adsorption of O_2, H_2, CO, NH_3, and NO_2 on ZnO nanotube: a density functional theory study, J. Phys. C 112 (2008) 5747–5755.
[31] D. Wang, X.F. Chu, M.L. Gong, Gas-sensing properties of sensors based on single-crystalline SnO_2 nanorods prepared by a simple molten-salt method, Sens. Actuators, B: Chem. 117 (2006) 183–187.
[32] Y.Z. Lv, C.R. Li, L. Guo, F.C. Wang, Y. Xu, X.F. Chu, Triethylamine gas sensor based on ZnO nanorods prepared by a simple solution route, Sens. Actuators, B: Chem. 141 (2009) 85–88.
[33] J. Zhang, X.H. Liu, S.H. Wu, B.Q. Cao, S.H. Zheng, One-pot synthesis of Au-supported ZnO nanoplates with enhanced gas sensor performance, Sens. Actuators, B: Chem. 169 (2012) 61–66.
[34] S.J. Kim, C.W. Na, I.S. Hwang, J.-H. Lee, One-pot hydrothermal synthesis of CuO–ZnO composite hollow spheres for selective H_2S detection, Sens. Actuators, B: Chem. 168 (2012) 83–89.
[35] Y. Liu, G.Z. Li, R. Mi, C.K. Deng, P.Z. Gao, An environment-benign method for the synthesis of p-NiO/n-ZnO heterostructure with excellent performance for gas sensing and photocatalysis, Sens. Actuators, B: Chem. 191 (2014) 537–544.
[36] H.-J. Kim, J.-H. Lee, Highly sensitive and selective gas sensors using p-type oxide semiconductors: overview, Sens. Actuators, B: Chem. 192 (2014) 607–627.
[37] J. Bandara, C.M. Divarathne, S.D. Nanayakkara, Fabrication of n–p junction electrodes made of n-type SnO_2 and p-type NiO for control of charge recombination in dye sensitized solar cells, Sol. Energy Mater. Sol. Cells 81 (2004) 429–437.
[38] Z.P. Li, Q.Q. Zhao, W.L. Fan, J.H. Zhan, Porous SnO_2 nanospheres as sensitive gas sensors for volatile organic compounds detection, Nanoscale 3 (2011) 1646–1652.
[39] H.C. Chiu, C.S. Yeh, Hydrothermal synthesis of SnO_2 nanoparticles and their gas-sensing of alcohol, J. Phys. Chem. C 111 (2007) 7256–7259.
[40] Y.J. Chen, L. Yu, D.D. Feng, M. Zhuo, M. Zhang, E.D. Zhang, Z. Xu, Q.H. Li, T.H. Wang, Superior ethanol-sensing properties based on Ni-doped SnO_2 p–n heterojunction hollow spheres, Sens. Actuators, B: Chem. 166–167 (2012) 61–67.
[41] Z.J. Wang, Z.Y. Li, J.H. Sun, H.N. Zhang, W. Wang, W. Zheng, C. Wang, Improved hydrogen monitoring properties based on p-NiO/n-SnO_2 heterojunction composite nanofibers, J. Phys. Chem. C 114 (2010) 6100–6105.

[42] X.H. Liu, J. Zhang, X.Z. Guo, S.H. Wu, S.R. Wang, Enhanced sensor response of Ni-doped SnO_2 hollow spheres, Sens. Actuators, B: Chem. 152 (2011) 162–167.
[43] L.L. Wang, J.N. Deng, T. Fei, T. Zhang, Template-free synthesized hollow NiO–SnO_2 nanospheres with high gas-sensing performance, Sens. Actuators, B: Chem. 164 (2012) 90–95.
[44] K.-Il. Choi, H.-J. Kim, Y.C. Kang, J.-H. Lee, Ultraselective and ultrasensitive detection of H_2S in highly humid atmosphere using CuO-loaded SnO_2 hollow spheres for real-time diagnosis of halitosis, Sens. Actuators, B: Chem. 194 (2014) 371–376.
[45] Y.L. Liu, G.Z. Li, R.D. Mia, C.K. Deng, P.Z. Gao, An environment-benign method for the synthesis of p-NiO/n-ZnO heterostructure with excellent performance for gas sensing and photocatalysis, Sens. Actuators, B: Chem. 191 (2014) 537–544.
[46] Z. Lou, L.L. Wang, T. Fei, T. Zhang, Enhanced ethanol sensing properties of NiO-doped SnO_2 polyhedra, New J. Chem. 36 (2012) 1003–1007.
[47] F. Shao, M.W.G. Hoffmann, J.D. Prades, R. Zamani, J. Arbiol, J.R. Morante, E. Varechkina, M. Rumyantseva, A. Gaskov, I. Giebelhaus, T. Fischer, S. Mathur, F. Hernández-Ramírez, Heterostructured p-CuO (nanoparticle)/n-SnO_2(nanowire) devices for selective H_2S detection, Sens. Actuators, B: Chem. 181 (2013) 130–135.
[48] L. Liu, C.C. Guo, S.C. Li, L.Y. Wang, Q.Y. Dong, W. Li, Improved H_2 sensing properties of Co-doped SnO_2 nanofibers, Sens. Actuators, B: Chem. 150 (2010) 806–810.
[49] Y.J. Hong, J.-W. Yoon, J.-H. Lee, Y.C. Kang, One-pot synthesis of Pd-loaded SnO_2 yolk–shell nanostructures for ultraselective methyl benzene sensors, Chem. A Eur. J. 20 (2014) 2737–2741.
[50] L.X. Zhang, J.H. Zhao, H.Q. Lu, L. Li, J.F. Zheng, J. Zhang, H. Li, Z.P. Zhu, Highly sensitive and selective dimethylamine sensors based on hierarchical ZnO architectures composed of nanorods and nanosheet-assembled microspheres, Sens. Actuators, B: Chem. 171–172 (2012) 1101–1109.
[51] D.E. Williams, Semiconducting oxides as gas-sensitive resistors, Sens. Actuators, B: Chem. 57 (1999) 1–16.
[52] Z.F. Dai, L. Xu, G.T. Duan, T. Li, H.W. Zhang, Y. Li, Y. Wang, Y.L. Wang, W.P. Cai, Fast-response, sensitive and low-powered chemosensors by fusing nanostructured porous thin film and IDEs-microheater chip, Sci. Rep. 3 (2013) 1669.
[53] X.F. Chu, D.L. Jiang, C.M. Zheng, The preparation and gas-sensing properties of $NiFe_2O_4$ nanocubes and nanorods, Sens. Actuators, B: Chem. 123 (2007) 793–797.
[54] S. Roy, S. Basu, ZnO thin film sensors for detecting dimethyl- and trimethylamine vapors, J. Mater. Sci.: Mater. Electron. 15 (2004) 321–326.
[55] T.H. Kwon, S.H. Park, J.Y. Ryu, H.H. Choi, Zinc oxide thin film doped with Al_2O_3, TiO_2 and V_2O_5 as sensitive sensor for trimethylamine gas, Sens. Actuators, B: Chem. 46 (1998) 75–79.

Biographies

Dianxing Ju is a graduate student focusing on ZnO semiconductor gas sensor for master degree at University of Jinan. He was awarded a B.Sc. degree in materials science and engineering from the same university in 2012.

Hongyan Xu is an Associate Professor at School of Materials Science and Engineering, University of Jinan. Her main research interests are the synthesis and fabrication of semiconductor nanomaterials and conductive polymer composite chemical gas sensors.

Jing Guo is a graduate student focusing on SnO_2 gas sensor and lithium battery for master degree at University of Jinan. She was awarded a B.Sc. degree in materials science and engineering from the same university in 2012.

Zhiwen Qiu is a graduate student focusing on PLD growth oxide film for Ph.D. degree at University of Jinan. She was awarded a B.Sc. degree in materials science and engineering from the same university in 2011.

Jun Zhang obtained his Ph.D. of Chemistry from Nankai University in 2011 and now is a lecturer with University of Jinan. His research is focused on nanomaterials and advanced applications in gas sensing and energy conversion devices.

Bingqiang Cao is a Professor with Taishan Scholar Chair for material physics with University of Jinan. His research group focuses on semiconducting oxide thin films, heterostructures, nanostructures, and related devices.